Lipopolysaccharide-Induced Activation of Human Monocytes

Bacterial lipopolysaccharide (serotype 0111:B4; Sigma) was added at 1 μg/mL to the cells as indicated for each experiment. NF-κB decoy at 5 μg/mL, NF-κB decoy-encapsulated NPs containing 0.1 mg/mL of PEG-PLGA NP and 5 μg/mL of NF-κB decoy, or the vehicle alone was added to the wells simultaneously. Four hours later, the cells were washed 3 times with PBS. NF-κB pathway activity was measured using a TransAM NF-κB p65 ELISA-based assay kit (Active Motif). Nuclear extracts of THP-1 were prepared with the NE-PER kit (Pierce) according to the manufacturer's protocol. All of the procedures were carried out at 4°C. Protein concentration was determined by BCA assay, and 20 μg of protein from each sample were used in the assay. Samples were placed along with 30 μL of binding buffer on a 96-well plate to which oligonucleotides containing an NF-κB consensus binding site had been immobilized. Plates were incubated for 1 hour on a shaker. During this time, the activated NF-κB contained in the sample specifically bound to this nucleotide. The plate was then washed, and the NF-κB complex bound to the oligonucleotides was detected using a primary antibody (100 μL diluted 1:1000 in antibody binding buffer for 1 hour) that is directed against the NF-κB p65 subunit. The plate was then washed again, 100 μL of secondary antibody (diluted 1:1000 in antibody binding buffer) conjugated to horseradish peroxidase was added, and the plate was incubated for 1 hour. The plate was washed again, and 100 μL of developing solution were added. The plate was incubated for 4 minutes away from direct light, 100 μL of stop solution were added, and the plate was read using a plate reader at 450 nm.

Human PASMC Proliferation Assay

Human PASMCs were seeded on 96-well culture plates at 1×10^4 cells per well (n=6 per group) in smooth muscle cells–basal medium with 10% FBS. After 24 hours, the cells were starved for 48 hours in serum-free medium to obtain quiescent nondividing cells. After starvation, 10% FBS was added. Also, a concentration of 1 mg/mL of NF-κB decoy only, NF-κB decoy-encapsulated PEG-PLGA NPs (0.05 mg/mL of PEG-PLGA and 1 mg/mL of decoy), or FITC-encapsulated PEG-PLGA NPs was added to each well. Cells were incubated for another 24 hours after addition of 5′-bromo-2′-deoxyuridine. 5′-Bromo-2′-deoxyuridine incorporation was evaluated by an ELISA kit from Calbiochem.

Statistical Analysis

All of the results are expressed as the mean±SEM. Statistical analysis of differences was performed by ANOVA followed by Bonferroni's multiple comparison test. The survival rates were determined by the Kaplan–Meier method. $P<0.05$ was considered statistically significant.

Results

Activation of NF-κB Expression in Patients With PA6H and in MCT-Induced PAH Rats

Localization of NF-κB activation was examined by immunohistochemical studies in lung tissue from patients using the antibody against α-p65.[9] An intense immunoreactivity of α-p65 was noted primarily in alveolar macrophages and to some extent in small pulmonary arterial lesions (mainly in smooth muscle cells in the medium) from 4 patients with PAH (Figure 1A and Figure S1A). This NF-κB activation was associated with positive staining of MCP-1 and IL-6. In contrast, none at all of α-p65 was detected in 2 control patients whose deaths were not attributed to lung disease (Figure S1B).

In MCT-induced PAH rats, activation NF-κB was noted mainly in alveolar macrophages and weakly in pulmonary artery lesions 7 days after MCT administration (Figure 1B and 1C). An electrophoretic mobility-shift assay was performed to detect the DNA binding activity of NF-κB (Figure S2). The binding activity of the lung increased in rats after MCT injection, which peaked on day 3 and decreased on day 7.

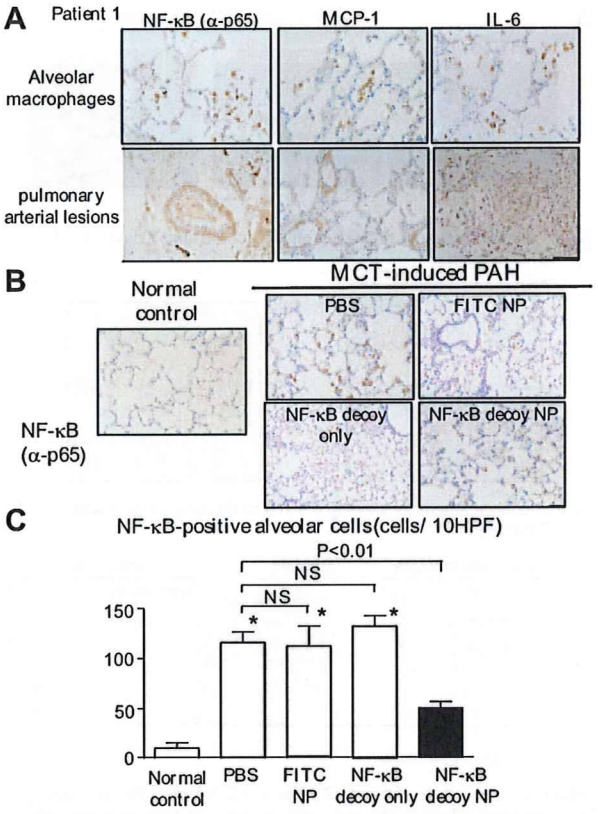

Figure 1. NF-κB activation in patients with PAH and rats with MCT-induced PAH and the effect of intratracheal instillation of NF-κB decoy NPs on NF-κB activation in rats. A, Micrographs of cross sections of the lung from patient 1 stained immunohistochemically with NF-κB (α-p65), MCP-1, and IL-6. Pictures stained with nonimmune IgG control are shown in the inset. Scale bar: 50 μm. B, Micrographs of cross sections of the lung stained immunohistochemically with NF-κB (α-p65) from normal rats and PAH rats 7 days after MCT injection. Scale bar: 50 μm. C, Effects of NF-κB decoy NPs on infiltration of NF-κB (α-p65)–positive cells 7 days after MCT injection. Data are mean±SEM (n=4 each). *$P<0.01$ vs PBS vs normal control.

Effects of Intratracheal Treatment With NF-κB Decoy NP on NF-κB Activation

Single intratracheal instillation of NF-κB decoy NPs, but not FITC NPs or NF-κB decoy only, resulted in marked attenuation of the increased NF-κB (α-p65) activity 7 days after MCT injection (Figure 1B and 1C). Treatment with NF-κB decoy NP markedly attenuated the DNA binding activity of NF-κB after MCT injection (Figure S2).

Because NF-κB was activated in alveolar monocytes and small pulmonary arterial smooth muscle cells in animals and humans with PAH, the effects of NF-κB decoy NPs on NF-κB activity were examined in the human monocyte cell line (THP-1) and in PASMCs in vitro (Figure S3). When those cultured cells were incubated with FITC-labeled NF-κB

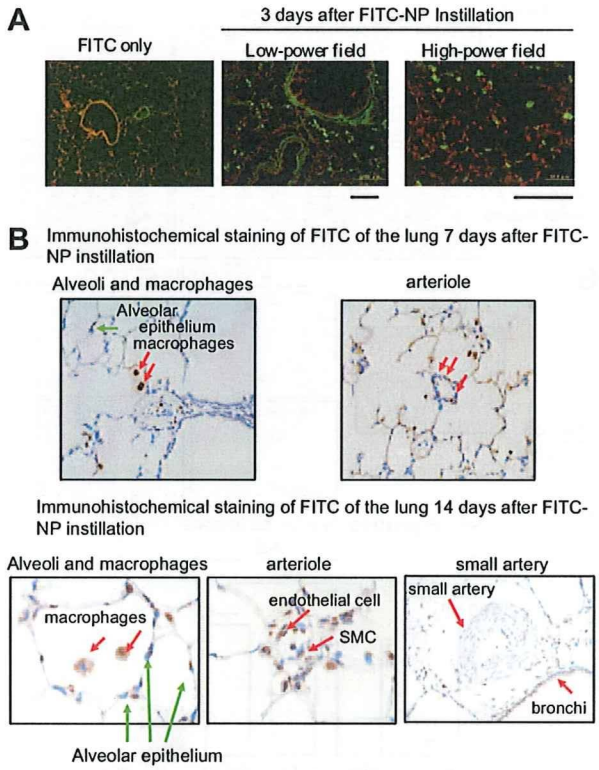

Figure 2. Localization of FITC after FITC-labeled NF-κB decoy NPs postinstillation in the rat lung. A, Fluorescent micrographs of cross sections from lung instillated with FITC only and FITC-labeled NF-κB decoy NPs on day 3 postinstillation. Nuclei were counterstained with propidium iodide (red). Scale bars: 100 μm. B, Micrographs of cross sections stained immunohistochemically against FITC from lung instillated intratracheally with FITC-NPs on days 7 and 14 postinstillation. Scale bars: 100 μm.

decoy NPs for 60 minutes, they were exclusively positive for intracellular localization of FITC. Treatment with NF-κB decoy NPs, but not but with FITC-NPs only or NF-κB decoy only, prevented NF-κB activation in THP-1 cells and attenuated proliferation of human PASMCs.

Localization of FITC-Labeled NF-κB Decoy NPs in the Lung of MCT-Induced PAH

Localization of FITC was examined after a single intratracheal instillation of FITC-labeled NF-κB decoy NPs in animals injected with MCT. Histopathologic examination of lung sections showed that strong FITC signals were detected only in FITC-NP–instillated lung 3 days after instillation, whereas no FITC signals were observed in control noninjected lungs or in lungs injected with FITC only (Figure 2A). There were the FITC-positive cells in bronchi and alveoli, alveolar macrophages, and small arteries. Immunofluorescent staining revealed FITC signals localized mainly in small arteries and arterioles, as well as in small bronchi and alveoli, 7 and 14 days after instillation of FITC-NPs (Figure 2B). FITC signals were not detected in remote organs (liver, spleen, kidney, and heart) on days 1, 3, and 7 (data not shown).

Effects of NF-κB Decoy NP on the Development of PAH in the Rat Model of MCT-Induced PAH

As reported previously by us and by other investigators,[5,16,17] the injection of MCT results in severe PAH (increased RV systolic pressure and RV hypertrophy; Figure 3) associated with small pulmonary arterial remodeling (Figure 4) and increased infiltration of ED-1–positive monocytes (Figure 4) 3 weeks after MCT injection. Single intratracheal treatment with NF-κB decoy NPs but not with NF-κB decoy only or FITC-NPs attenuated the development of PAH (Figure 3), small pulmonary arterial remodeling (Figure 4), and inflammation (Figure 4).

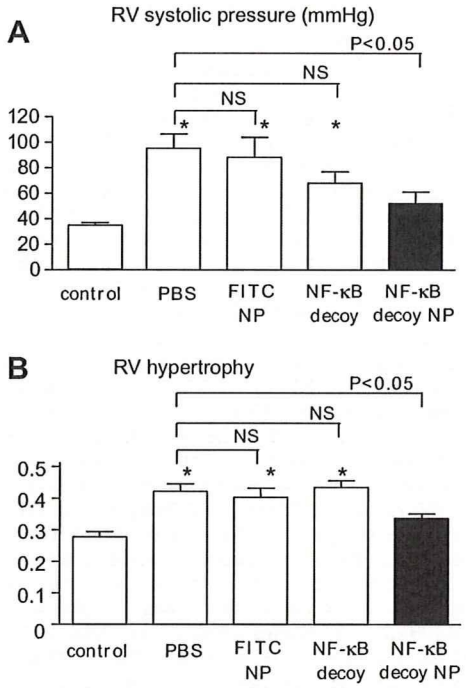

Figure 3. Effects of NF-κB decoy NPs on RV systolic pressure and RV hypertrophy 3 weeks after MCT injection. A, RV systolic pressure 21 days after MCT injection in 4 groups. Data are mean±SEM (n=6 each). *$P<0.05$ vs normal control. B, RV hypertrophy (the ratio of RV/[LV+S]) 21 days after MCT injection in the different treatment groups. Data are mean±SEM (n=6 each). *$P<0.05$ vs normal control.

Effects of NF-κB Decoy NPs on Expression of Proinflammatory Factors

As reported previously,[3,4] MCT-induced PAH was associated with increased gene expression of proinflammatory factors. Treatment with NF-κB decoy NPs significantly reduced the increased gene expression of MCP-1, TNF-α, and IL-1β (Figure 5). NF-κB decoy NPs tended to decrease the expression of IL-6 and intercellular adhesion molecule-1.

In Vitro NP Release Kinetics

An analysis of the in vitro FITC release kinetics from FITC-NP showed an early burst of FITC release such that ≈40% of the total amount ultimately released was present on day 1, followed by sustained release of the remaining FITC over the next 28 days (Figure S4).

Effects of NF-κB Decoy NPs on Survival

Treatment with NF-κB decoy NPs 21 days after MCT injection significantly ($P<0.01$) improved the survival rate (Figure 6).

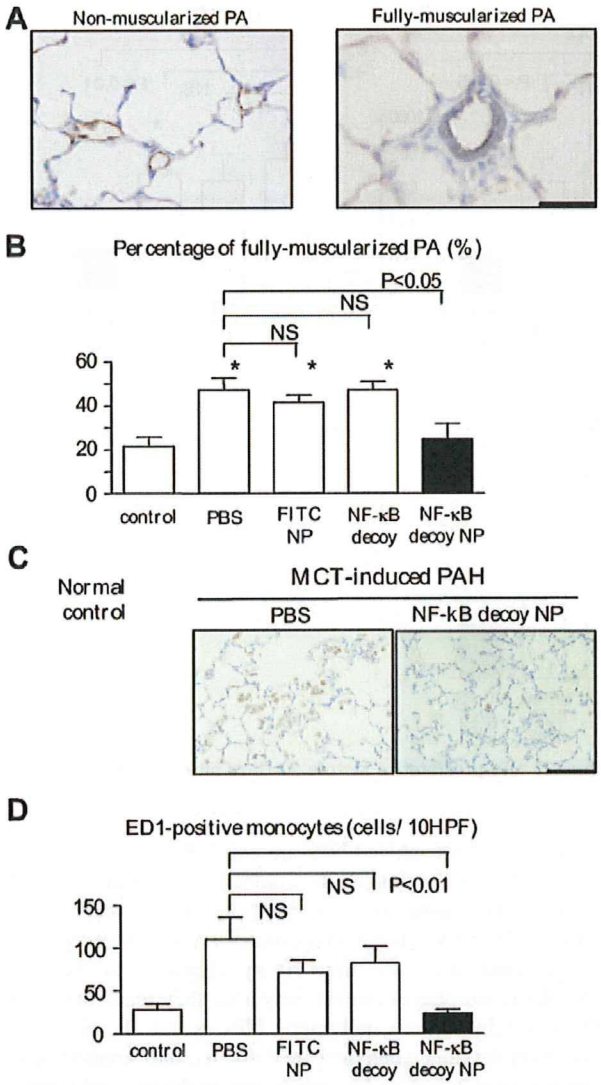

Figure 4. Effects of NF-κB decoy NPs on small pulmonary arterial remodeling and infiltration of monocytes. A, Representative micrographs of nonmuscularized and fully muscularized small pulmonary arteries stained immunohistochemically against the endothelial layer (brown) and medial smooth muscle cells (blue). Scale bar: 50 μm. B, The percentage of fully muscularized small pulmonary arteries in the different treatment groups. Data are mean±SEM (n=6 each). *$P<0.05$ vs normal control. C, Representative micrographs of pulmonary alveoli stained immunohistochemically for ED-1–positive monocytes. Scale bar: 50 μm. D, Infiltration of ED-1–positive monocytes into the lung (the number of positive cells per 10 high-power field cross sections). Data are mean±SEM (n=6 each). *$P<0.01$ vs normal control.

Discussion

The present study demonstrates for the first time that intratracheal instillation of PEG-PLGA NPs is an excellent system for drug delivery of NF-κB decoy to the lung. The FITC signals were detected not only in small bronchial tracts but also in alveolar macrophages and small pulmonary arteries for ≤14 days after a single instillation. After cellular uptake of NPs, NPs might slowly release encapsulated decoy into the cytoplasm as PLGA is hydrolyzed. This might protect the encapsulated decoy from intracellular degradation before its arrival at the nuclear target. Our in vitro studies in cultured human monocytes and pulmonary arterial smooth muscle cells support this notion. Therefore, this platform nanotechnology may represent a novel NP-mediated drug delivery system for treatment of severe lung diseases, including PAH.

The present study also reports a pivotal role of NF-κB in the pathogenesis of PAH. Recently, Sawada et al[19] and Huang et al[20] reported that systemic daily administration of pyrrolidine dithiocarbamate, a nonspecific inhibitor of NF-κB, attenuated the development of MCT-induced PAH. Pyrrolidine dithiocarbamate is known to be a low molecular weight thiol compound and has anti-inflammatory and antioxidant activity independent of the NF-κB pathway. Indeed, in a study by Huang et al,[20] pyrrolidine dithiocarbamate treatment had no effect on MCT-induced NF-κB activation. In contrast, we found in the present study that NF-κB is activated in alveolar macrophages and small pulmonary arteries associated with NF-κB–dependent inflammatory factors (eg, MCP-1, IL-1, and TNF-α) in patients with PAH and rats with MCT-induced PAH, and blockade of NF-κB activation by a single intratracheal instillation of NF-κB decoy NPs reduced inflammatory changes. These data suggest that NF-κB might be pivotal in mediating inflammatory changes seen in PAH.

We also found that intratracheal instillation of NF-κB decoy NPs prevented the development of PAH (increased RV pressure, RV hypertrophy, and pulmonary artery remodeling) in the prevention protocol. We and others have reported that blockade of MCP-1 reduces vascular pathology after vascular injury[9,21–25] and the development of PAH.[5,6] In addition, as we reported in human coronary artery smooth muscle cells in vitro,[12,26] we found that NF-κB decoy NPs attenuated proliferation of human PASMCs in vitro. Therefore, the beneficial effects of NF-κB decoy NPs can be attributable to inhibition of inflammation and smooth muscle cell proliferation resulting from reduced NF-κB activation.

Furthermore, we found that a single intratracheal treatment of NF-κB decoy NPs 3 weeks after MCT injection improved survival rate in the treatment protocol, suggesting that this NP-mediated NF-κB decoy delivery may have significant therapeutic effects. We did not examine the therapeutic effects of repetitive intratracheal instillation of NF-κB decoy NPs, because it is technically difficult to perform multiple intratracheal instillation of this NP system in rats and other small animals. For translation of our present findings into clinical medicine, further studies are needed to investigate whether repetitive delivery of NPs into lungs produces greater therapeutic effects over time.

Several points are worth mentioning with regard to potential clinical applicability. First, from a toxicological point of view, no adverse reactions, eg, pulmonary inflammation, after exposure to a single intratracheal instillation of FITC-NPs (PEG-PLGA at 1 mg per body) or NF-κB decoy NPs (NF-κB decoy at 50 μg per body in rats weighing 250 to 300 g) were noted in the rat model, suggesting that the NPs used in this study may not cause an adverse reaction. However, the 3-week observation period for this NP system might be too short to determine its safety. Second, we reported recently that neither intravenous injection of the NF-κB decoy at 1 mg per body in monkeys nor deployment

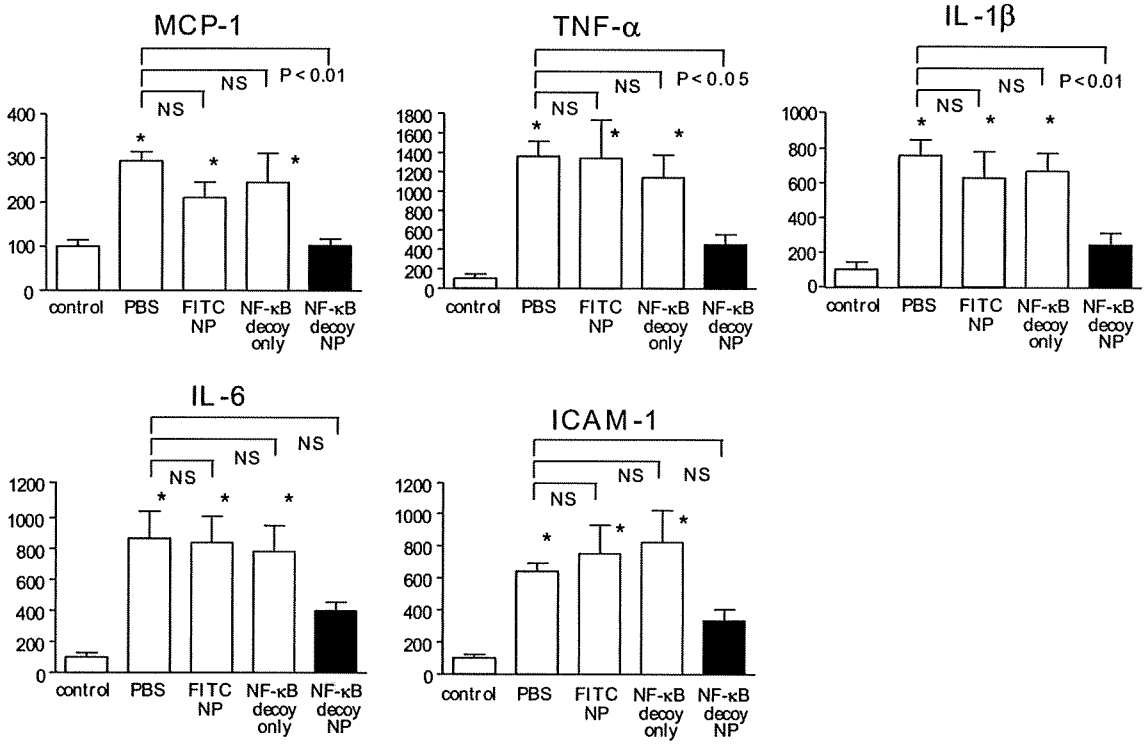

Figure 5. Effects of NF-κB decoy NPs on mRNA levels of various inflammatory and proliferative factors 21 days after MCT injection (n=5 each). *$P<0.01$ vs normal control.

of an NF-κB decoy-eluting stent (≈600 μg per stent) in rabbits showed systemic adverse effects.[12] More important are the findings of a clinical trial that we completed recently to test the feasibility and safety of the NF-κB decoy. The decoy was transfected into the stented coronary artery sites at doses of 1000, 2000, or 4000 μg per body via a channel balloon catheter immediately after successful percutaneous coronary intervention in 18 patients with flow-limiting coronary stenosis.[27] The patients showed low restenosis rates and no evidence of systemic adverse effects during the 6-month observation period. These data support the notion that NF-κB decoy can be applied in a clinical setting. Third, this NP system itself is not suitable for inhalant therapy, because it is known that most inhaled NPs are exhaled rather than being delivered into the lung.[28] In contrast, microparticles with aerodynamic diameters between 2 and 8 μm reach small bronchi. However, the microparticles are easily recognized and eliminated by the mucociliary clearance system and alveolar macrophages immediately after they reach the small bronchi.[28] In contrast, polymeric NPs escape the clearance system of the lung when they are delivered into small bronchi and are, thus, taken up by alveoli, macrophages, and pulmonary small vessels. Therefore, to use this NP system for inhalant therapy, we need to develop the nanocomposite microsized particles[28] that will decompose to NPs after reaching the small bronchi.

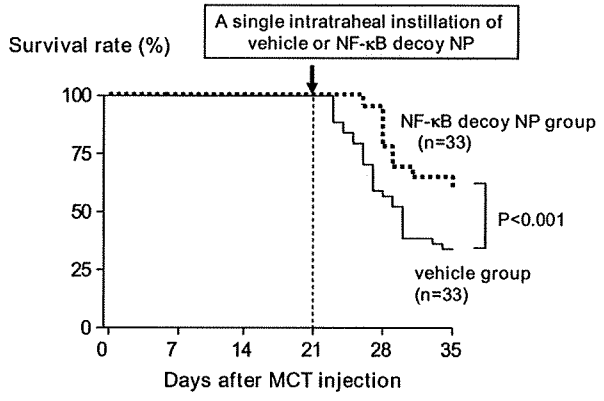

Figure 6. Effects of NF-κB decoy NPs on survival rate. Survival rate analyzed by the Kaplan–Meier method in vehicle and NF-κB decoy NP groups.

Perspectives

This study has shown that NF-κB is activated in pulmonary arterial lesions in patients with PAH and in rats with MCT-induced PAH, and blockade of NF-κB by NP-mediated NF-κB decoy delivery not only prevented the development of MCT-induced PAH in the prevention protocol but also improved survival rate in the treatment protocol. These data support the notion that NF-κB plays a pivotal role in the pathogenesis of PAH and, thus, represents a new therapeutic target for PAH. This nanotechnology platform may be developed as a more effective and less invasive nanomedicine in PAH therapy.

Sources of Funding

This study was supported by Grants-in-Aid for Scientific Research (19390216 and 19650134) from the Ministry of Education, Science, and Culture (Tokyo, Japan) and by Health Science Research grants

(Research on Translational Research and Nano-medicine) from the Ministry of Health, Labor, and Welfare (Tokyo, Japan).

Disclosures

K.E. and R.M. hold a patent on the results reported in this study. The remaining authors report no conflicts.

References

1. Farber HW, Loscalzo J. Pulmonary arterial hypertension. *N Engl J Med.* 2004;351:1655–1665.
2. Humbert M, Sitbon O, Simonneau G. Treatment of pulmonary arterial hypertension. *N Engl J Med.* 2004;351:1425–1436.
3. Stenmark KR, Fagan KA, Frid MG. Hypoxia-induced pulmonary vascular remodeling: cellular and molecular mechanisms. *Circ Res.* 2006; 99:675–691.
4. Sanchez O, Marcos E, Perros F, Fadel E, Tu L, Humbert M, Dartevelle P, Simonneau G, Adnot S, Eddahibi S. Role of endothelium-derived CC chemokine ligand 2 in idiopathic pulmonary arterial hypertension. *Am J Respir Crit Care Med.* 2007;176:1041–1047.
5. Ikeda Y, Yonemitsu Y, Kataoka C, Kitamoto S, Yamaoka T, Nishida K, Takeshita A, Egashira K, Sueishi K. Anti-monocyte chemoattractant protein-1 gene therapy attenuates pulmonary hypertension in rats. *Am J Physiol Heart Circ Physiol.* 2002;283:H2021–H2028.
6. Kimura H, Kasahara Y, Kurosu K, Sugito K, Takiguchi Y, Terai M, Mikata A, Natsume M, Mukaida N, Matsushima K, Kuriyama T. Alleviation of monocrotaline-induced pulmonary hypertension by antibodies to monocyte chemotactic and activating factor/monocyte chemoattractant protein-1. *Lab Invest.* 1998;78:571–581.
7. Katsushi H, Kazufumi N, Hideki F, Katsumasa M, Hiroshi M, Kengo K, Hiroshi D, Nobuyoshi S, Tetsuro E, Hiromi M, Tohru O. Epoprostenol therapy decreases elevated circulating levels of monocyte chemoattractant protein-1 in patients with primary pulmonary hypertension. *Circ J.* 2004;68:227–231.
8. Itoh T, Nagaya N, Ishibashi-Ueda H, Kyotani S, Oya H, Sakamaki F, Kimura H, Nakanishi N. Increased plasma monocyte chemoattractant protein-1 level in idiopathic pulmonary arterial hypertension. *Respirology.* 2006;11:158–163.
9. Brand K, Page S, Rogler G, Bartsch A, Brandl R, Knuechel R, Page M, Kaltschmidt C, Baeuerle PA, Neumeier D. Activated transcription factor nuclear factor-kappa B is present in the atherosclerotic lesion. *J Clin Invest.* 1996;97:1715–1722.
10. Morishita R, Higaki J, Tomita N, Ogihara T. Application of transcription factor "decoy" strategy as means of gene therapy and study of gene expression in cardiovascular disease. *Circ Res.* 1998;82:1023–1028.
11. Kitamoto S, Egashira K, Kataoka C, Koyanagi M, Katoh M, Shimokawa H, Morishita R, Kaneda Y, Sueishi K, Takeshita A. Increased activity of nuclear factor-kappaB participates in cardiovascular remodeling induced by chronic inhibition of nitric oxide synthesis in rats. *Circulation.* 2000; 102:806–812.
12. Ohtani K, Egashira K, Nakano K, Zhao G, Funakoshi K, Ihara Y, Kimura S, Tominaga R, Morishita R, Sunagawa K. Stent-based local delivery of nuclear factor-kappaB decoy attenuates in-stent restenosis in hypercholesterolemic rabbits. *Circulation.* 2006;114:2773–2779.
13. Murakami H, Kobayashi M, Takeuchi H, Kawashima Y. Preparation of poly(DL-lactide-co-glycolide) nanoparticles by modified spontaneous emulsification solvent diffusion method. *Int J Pharm.* 1999;187:143–152.
14. Kawashima Y, Yamamoto H, Takeuchi H, Hino T, Niwa T. Properties of a peptide containing DL-lactide/glycolide copolymer nanospheres prepared by novel emulsion solvent diffusion methods. *Eur J Pharm Biopharm.* 1998;45:41–48.
15. Panyam J, Zhou WZ, Prabha S, Sahoo SK, Labhasetwar V. Rapid endo-lysosomal escape of poly(DL-lactide-co-glycolide) nanoparticles: implications for drug and gene delivery. *FASEB J.* 2002;16:1217–1226.
16. Schermuly RT, Dony E, Ghofrani HA, Pullamsetti S, Savai R, Roth M, Sydykov A, Lai YJ, Weissmann N, Seeger W, Grimminger F. Reversal of experimental pulmonary hypertension by PDGF inhibition. *J Clin Invest.* 2005;115:2811–2821.
17. Cowan KN, Heilbut A, Humpl T, Lam C, Ito S, Rabinovitch M. Complete reversal of fatal pulmonary hypertension in rats by a serine elastase inhibitor. *Nat Med.* 2000;6:698–702.
18. Quinlan TR, Li D, Laubach VE, Shesely EG, Zhou N, Johns RA. eNOS-deficient mice show reduced pulmonary vascular proliferation and remodeling to chronic hypoxia. *Am J Physiol Lung Cell Mol Physiol.* 2000;279:L641–L650.
19. Sawada H, Mitani Y, Maruyama J, Jiang BH, Ikeyama Y, Dida FA, Yamamoto H, Imanaka-Yoshida K, Shimpo H, Mizoguchi A, Maruyama K, Komada Y. A nuclear factor-kappaB inhibitor pyrrolidine dithiocarbamate ameliorates pulmonary hypertension in rats. *Chest.* 2007;132: 1265–1274.
20. Huang J, Kaminski PM, Edwards JG, Yeh A, Wolin MS, Frishman WH, Gewitz MH, Mathew R. Pyrrolidine dithiocarbamate restores endothelial cell membrane integrity and attenuates monocrotaline-induced pulmonary artery hypertension. *Am J Physiol Lung Cell Mol Physiol.* 2008;294: L1250–L1259.
21. Egashira K. Molecular mechanisms mediating inflammation in vascular disease: special reference to monocyte chemoattractant protein-1. *Hypertension.* 2003;41:834–841.
22. Egashira K. Clinical importance of endothelial function in arteriosclerosis and ischemic heart disease. *Circ J.* 2002;66:529–533.
23. Ohtani K, Usui M, Nakano K, Kohjimoto Y, Kitajima S, Hirouchi Y, Li XH, Kitamoto S, Takeshita A, Egashira K. Antimonocyte chemoattractant protein-1 gene therapy reduces experimental in-stent restenosis in hypercholesterolemic rabbits and monkeys. *Gene Ther.* 2004;11: 1273–1282.
24. Usui M, Egashira K, Ohtani K, Kataoka C, Ishibashi M, Hiasa K, Katoh M, Zhao Q, Kitamoto S, Takeshita A. Anti-monocyte chemoattractant protein-1 gene therapy inhibits restenotic changes (neointimal hyperplasia) after balloon injury in rats and monkeys. *FASEB J.* 2002;16: 1838–1840.
25. Egashira K, Zhao Q, Kataoka C, Ohtani K, Usui M, Charo IF, Nishida K, Inoue S, Katoh M, Ichiki T, Takeshita A. Importance of monocyte chemoattractant protein-1 pathway in neointimal hyperplasia after periarterial injury in mice and monkeys. *Circ Res.* 2002;90:1167–1172.
26. Lemarie CA, Esposito B, Tedgui A, Lehoux S. Pressure-induced vascular activation of nuclear factor-kappaB: role in cell survival. *Circ Res.* 2003; 93:207–212.
27. Egashira K, Suzuki J, Ito H, Aoki M, Isobe M, Morishita R. Long-term follow up of initial clinical cases with NF-kappaB decoy oligodeoxynucleotide transfection at the site of coronary stenting. *J Gene Med.* 2008; 10:805–809.
28. Tomoda K, Ohkoshi T, Kawai Y, Nishiwaki M, Nakajima T, Makino K. Preparation and properties of inhalable nanocomposite particles: effects of the temperature at a spray-dryer inlet upon the properties of particles. *Colloids Surf B Biointerfaces.* 2008;61:138–144.

A Journal of the American College of Cardiology

April 2009
Volume 2, No. 4

JACC cardiovascular Interventions

- Pulmonary Vein Stenosis Complicating Ablation for AF

MINI-FOCUS: Stent Technology

- Bioabsorbable Polymeric Nanoparticle-Eluting Stents
- Lowering the Dose of Sirolimus Reduces Delayed Healing
- Antirestenotic Efficacy in DES With and Without Polymer
- Biodegradable-Polymer Coated SES in "Real-World" Practice
- IVUS and Angiography Following Bioabsorbable Magnesium Stents

- Drug-Eluting and Bare-Metal Stents for Stable CAD
- Impact of DES vs. BMS on Mortality in Patients With Anemia
- Pre-Hospital ECGs and STEMI Receiving Center Networks
- Predictors and Outcomes of Ad Hoc vs. Non-Ad Hoc PCI
- Predictors of MACE and Optimal Post-Stent FFR After BMS

(A) Light and fluorescence stereomicroscopy of fluorescein-isothiocyanate–incorporated nanoparticle-eluting stent. (B) Scanning electron microscopy (low and high magnification). See page 279.

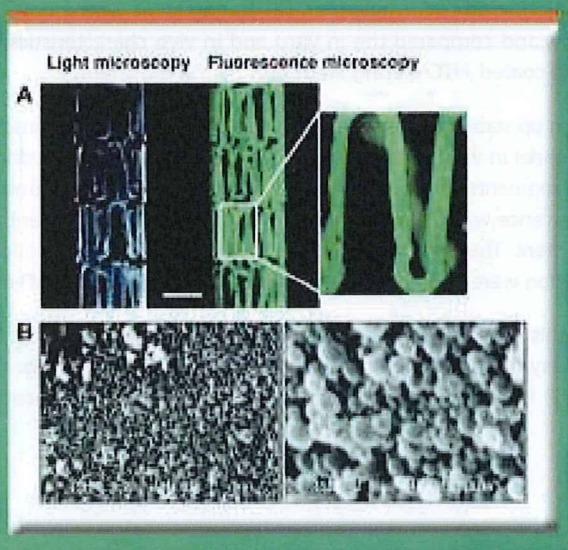

ELSEVIER

ISSN 1936-8798

www.jacc-interventions.org

JACC: CARDIOVASCULAR INTERVENTIONS
© 2009 BY THE AMERICAN COLLEGE OF CARDIOLOGY FOUNDATION
PUBLISHED BY ELSEVIER INC.

VOL. 2, NO. 4, 2009
ISSN 1936-8798/09/$36.00
DOI: 10.1016/j.jcin.2008.08.023

MINI-FOCUS: STENT TECHNOLOGY

Formulation of Nanoparticle-Eluting Stents by a Cationic Electrodeposition Coating Technology

Efficient Nano-Drug Delivery via Bioabsorbable Polymeric Nanoparticle-Eluting Stents in Porcine Coronary Arteries

Kaku Nakano, PHD,* Kensuke Egashira, MD, PHD,* Seigo Masuda, MD,* Kouta Funakoshi, MD,* Gang Zhao, MD, PHD,§ Satoshi Kimura, MD,† Tetsuya Matoba, MD, PHD,* Katsuo Sueishi, MD, PHD,‡ Yasuhisa Endo, PHD,¶ Yoshiaki Kawashima, PHD,‖ Kaori Hara, PHD,# Hiroyuki Tsujimoto, PHD,# Ryuji Tominaga, MD, PHD,† Kenji Sunagawa, MD, PHD*

Fukuoka, Aichi, Kyoto, and Osaka, Japan; and Shanghai, China

Objectives The objective of this study was to formulate a nanoparticle (NP)-eluting drug delivery stent system by a cationic electrodeposition coating technology.

Background Nanoparticle-mediated drug delivery systems (DDS) are poised to transform the development of innovative therapeutic devices. Therefore, we hypothesized that a bioabsorbable polymeric NP-eluting stent provides an efficient DDS that shows better and more prolonged delivery compared with dip-coating stent.

Methods We prepared cationic NP encapsulated with a fluorescence marker (FITC) by emulsion solvent diffusion method, succeeded to formulate an NP-eluting stent with a novel cation electrodeposition coating technology, and compared the in vitro and in vivo characteristics of the FITC-loaded NP-eluting stent with dip-coated FITC-eluting stent and bare metal stent.

Results The NP was taken up stably and efficiently by cultured vascular smooth muscle cells in vitro. In a porcine coronary artery model in vivo, substantial FITC fluorescence was observed in neointimal and medial layers of the stented segments that had received the FITC-NP-eluting stent until 4 weeks. In contrast, no substantial FITC fluorescence was observed in the segments from the polymer-based FITC-eluting stent or from bare metal stent. The magnitudes of stent-induced injury, inflammation, endothelial recovery, and neointima formation were comparable between bare metal stent and NP-eluting stent groups.

Conclusions Therefore, this NP-eluting stent is an efficient NP-mediated DDS that holds as an innovative platform for the delivery of less invasive nano-devices targeting cardiovascular disease. (J Am Coll Cardiol Intv 2009;2:277–83) © 2009 by the American College of Cardiology Foundation

From the Departments of *Cardiovascular Medicine, †Cardiovascular Surgery, and ‡Pathology, Graduate School of Medical Sciences, Kyushu University, Fukuoka, Japan; §Department of Cardiovascular Medicine, 6th People's Hospital, Shanghai Jiaotong University, Shanghai, China; ‖School of Pharmaceutical Science, Aichi Gakuin University, Aichi, Japan; ¶Division of Applied Biology, Kyoto Institute of Technology, Kyoto, Japan; and the #Hosokawa Powder Technology Research Institute, Osaka, Japan.
This study was supported by Grants-in-Aid for Scientific Research (19390216, 19650134) from the Ministry of Education, Science, and Culture, Tokyo, Japan; Health Science Research Grants (Research on Translational Research and Nano-medicine) from the Ministry of Health, Labor, and Welfare, Tokyo, Japan; and the Program for Promotion of Fundamental Studies in Health Sciences of the Organization for Pharmaceutical Safety and Research, Tokyo, Japan. Dr. Egashira holds a patent on the results reported in this present study. Drs Nakano and Egashira contributed equally to this work.

Manuscript received July 29, 2008, accepted August 22, 2008.

JACC: CARDIOVASCULAR INTERVENTIONS, VOL. 2, NO. 4, 2009
APRIL 2009:277–83

In the 3 years since they were introduced for clinical use, polymer-based drug-eluting stents (DES) that carry antiproliferative drugs such as sirolimus or paclitaxel, have been used extensively in percutaneous coronary interventions for the prevention of restenosis (1–3). Through the effects of these antiproliferation agents on vascular smooth muscle cells (VSMCs) and inflammatory cells, DES can reduce the rate of restenosis and target-vessel revascularization to below 10%. However, the increased risk of late in-stent thrombosis (resulting in acute myocardial infarction and death) associated with use of the first-generation DES devices has become a major issue (4). In particular, the off-label use of DES for complex coronary lesions (long and diffuse lesions, left main lesions, culprit lesion of acute coronary syndrome, and so forth) increases the risk of late in-stent thrombosis (5,6). These adverse effects are thought to result mainly from the antiproliferative effects of the drugs on the endothelial cells, leading to impaired arterial healing processes (impaired endothelial regeneration, excessive inflammation, proliferation, and fibrin deposition) and partly from the use of nonbiocompatible polymers in stent construction (7–9). Clearly, a novel DES system with fewer associated adverse effects is needed.

Abbreviations and Acronyms

DDS = drug delivery system
DES = drug-eluting stent(s)
FITC = fluorescein isothiocyanate
NP = nanoparticle(s)
PLGA = poly (DL-lactide-*co*-glycolide)
VSMC = vascular smooth muscle cell

Current DES polymer-coating technology uses dip- and/or spray-coating methodology. These methods are useful for coating stents with strongly lipophilic drugs such as sirolimus but not for water-soluble drugs or deoxyribonucleic acid (DNA). Recently, we and others reported the formulation of plasmid DNA- or oligonucleotide-coated stents with a water-soluble polymer, which showed limited delivery efficacy and non optimal therapeutic effects for clinical application (10–13). The application of nanotechnology-based drug delivery system (DDS) is expected to have a major impact on the development of efficient and safe DDS.(14) Previously, we reported the development of such a DDS, a polymeric nanoparticle (NP) formulated from the biodegradable polymer poly (DL-lactide-*co*-glycolide) (PLGA) (15,16) that can entrap hydrophilic agents (protein, oligonucleotide, DNA, and the like), penetrate cellular membrane via endocytosis, and deliver the encapsulated therapeutic agents into the cellular cytoplasm. The PLGA hydrolyzes slowly, is metabolized, and is eliminated from the body. The PLGA NP offers the advantages of efficient intracellular delivery of different classes of therapeutic agents and the capacity for sustained intracytoplasmic release (17). Until now, no existing technology could produce an active coating of NP on the surface of metallic stents.

We have formulated a bioabsorbable polymeric NP-eluting stent with a novel cation electrodeposition coating technology. We hypothesized that this NP-eluting stent system would be an efficient innovative platform for in vivo drug delivery. The aims of this study were to: 1) formulate a bioabsorbable polymeric NP-eluting metallic stent with cation electrodeposition NP coating technology; 2) characterize the in vitro kinetics of drug release from NP and the cellular uptake and localization of NP; and 3) evaluate the feasibility of using NP-eluting stents in vivo in porcine coronary arteries.

Methods

Preparation of cationic PLGA NP with chitosan-mediated surface modification. Cationic PLGA NP encapsulated with fluorescein-isothiocyanate (FITC) were prepared by a previously reported emulsion solvent diffusion method in purified water (15,16). Additional details are provided in the Online Appendix.

Preparation of NP-eluting stents by cationic electrodeposition coating technology. Cationic electrodeposition coating was prepared in NP solution at a concentration of 50 mg/ml in distilled water and deposited on cathodic, 15-mm stainless-steel, balloon-expandable stents (Multilink, Guidant, Indianapolis, Indiana) with current maintained at 2.0 mA by a direct current power supply (Nippon Stabilizer Co., Tokyo, Japan) for different periods under sterile conditions (Online Fig. III). This electrodeposition coating procedure produced a coating of approximately 654.0 ± 167.5 μg (n = 12) of NP/stent and 31 ± 2 μg of FITC/stent (n = 12). Additional details are provided in the Online Appendix.

Measurement of in vitro NP release kinetics. To measure FITC release kinetics, FITC-NP (n = 8) was immersed in Tris-EDTA buffer, and the released FITC from NP was measured. The FITC-NP–eluting stents (n = 8) were also immersed in Tris-EDTA buffer, and the eluted FITC-containing NP was measured.

Cellular uptake and intracellular distribution of NP. Human coronary artery smooth muscle cells (SMCs) were used to perform this study. Additional details are provided in the Online Appendix.

Cytotoxicity assay. The cytotoxicity of PLGA NP on human coronary artery SMCs was determined with an MTS assay (Promega, Dojin, Japan). Additional details are provided in the Online Appendix.

Animal preparation, stent implantation, and coronary angiography. Domestic male pigs (weighing 25 to 30 kg) were anesthetized and divided into 3 groups that received noncoated bare metal stents (1 week, n = 3; 2 week, n = 3; 4 week, n = 8; 6 week, n = 3), FITC-incorporated NP-eluting stents (2 week, n = 3; 2 week, n = 3; 4 week, n = 8; 6 week, n = 3), or dip-coated stents with thin layers of PLGA polymer containing FITC (1 week; n = 3, 2 week; n = 3, 4 week; n = 3), to either the left anterior descending

or the left circumflex coronary artery. Animals were killed after 1, 2, 4, or 6 weeks, and the stented arterial sites and contralateral non stented sites were excised for biochemical, immunohistochemical, and morphometric analyses. Left coronary angiography was performed before, immediately after, and 4 weeks after stent implantation. Additional details are provided in the Online Appendix.

Histopathological studies. The stented arterial segment at 4 weeks after stent implantation was divided into 2 parts at the center of the stent, and the proximal part was embedded in resinoid. The distal part of the stent was used for either fluorescence or pathological analysis after the stent struts were gently removed with micro-forceps. Additional details are provided in the Online Appendix.

Statistical analysis. Data are expressed as mean ± SEM. The statistical analysis of differences between 2 groups was performed with the unpaired t test. The analysis of differences among 3 groups was compared by 1-way analysis of variance. Values of $p < 0.05$ were considered to be statistically significant.

Results

Fabrication of NP-eluting stent and NP release kinetics in vitro. The cationic electrodeposit coating formed a thin and uniform layer of NP on the surface of stents without webbing between the struts (Fig. 1A). Interestingly, amount of coating of NP on the stent surface increased with period of electricity (Online Fig. III).

Light and fluorescence microscopy analysis revealed that the polymer stretched after balloon expansion, but no fragmentation was observed (Fig. 1A). Scanning electron microscopy analysis revealed that NP was structurally intact and cohesive (Fig. 1B). An analysis of the in vitro FITC release kinetics from FITC-NP showed an early burst of FITC release such that approximately 40% of the total amount ultimately released was present on day 1, followed by sustained release of the remaining FITC over the next 30 days (Fig. 1C). The in vitro FITC release kinetics from NP-eluting stents also showed a similar release pattern (Fig. 1D).

In vitro cell uptake and intracellular distribution of NP. Incubation of human coronary artery SMCs with FITC-loaded NP (0.1 mg/ml PLGA) showed highly efficient and stable intracellular delivery of NP (Fig. 2A). In contrast, no fluorescence was detected when the SMCs were incubated with blank NP or FITC only. Fluorescence confocal microscopy revealed that: 1) the SMCs took up the NP rapidly, and NP remained stable in the cell for at least 24 h of incubation; and 2) NP was seen in both the nuclei and the cytoplasm (Figs. 2B and 2C). Transmission electron microscopy of the cellular cross-sections revealed the intracellular localization of NP at 24 h of incubation (Fig. 2D). Furthermore, NP eluted from the FITC-NP-eluting stent was added to human coronary artery SMCs and incubated

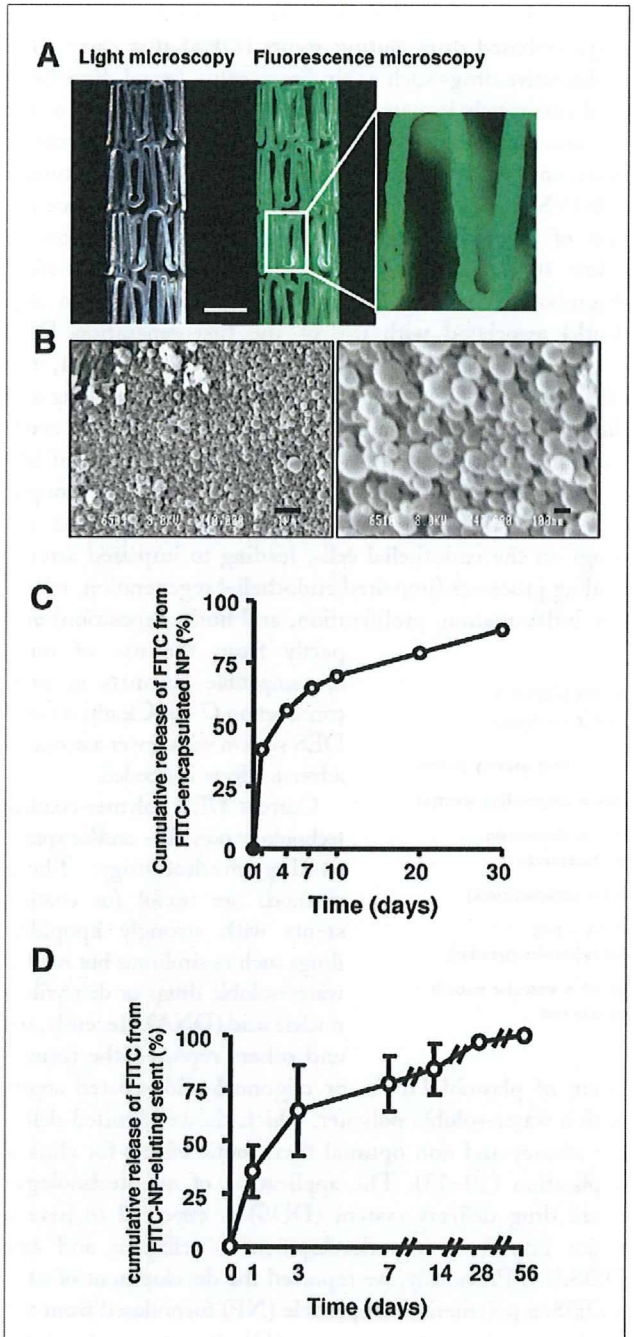

Figure 1. Formulation of FITC-Encapsulated NP-Eluting Stents by a Cationic Electrodeposition Coating Technology

(A) Light and fluorescence stereomicroscopy photograph of balloon-expanded fluorescein-isothiocyanate (FITC)-incorporated nanoparticle (NP)-eluting stent. **Scale bar** = 1 mm. **(B)** Scanning electron microscopy photograph (**left**: low magnification, **scale bar** = 1 μm; **right**: high magnification; **scale bar** = 100 nm) of balloon-expanded NP-eluting stent. **(C, D)** In vitro time course of cumulative FITC release from the FITC-incorporated NP and FITC-incorporated NP release from the NP-eluting stents (n = 8 each). The percentage of incremental quantities of released FITC was plotted against time.

JACC: CARDIOVASCULAR INTERVENTIONS, VOL. 2, NO. 4, 2009
APRIL 2009:277–83

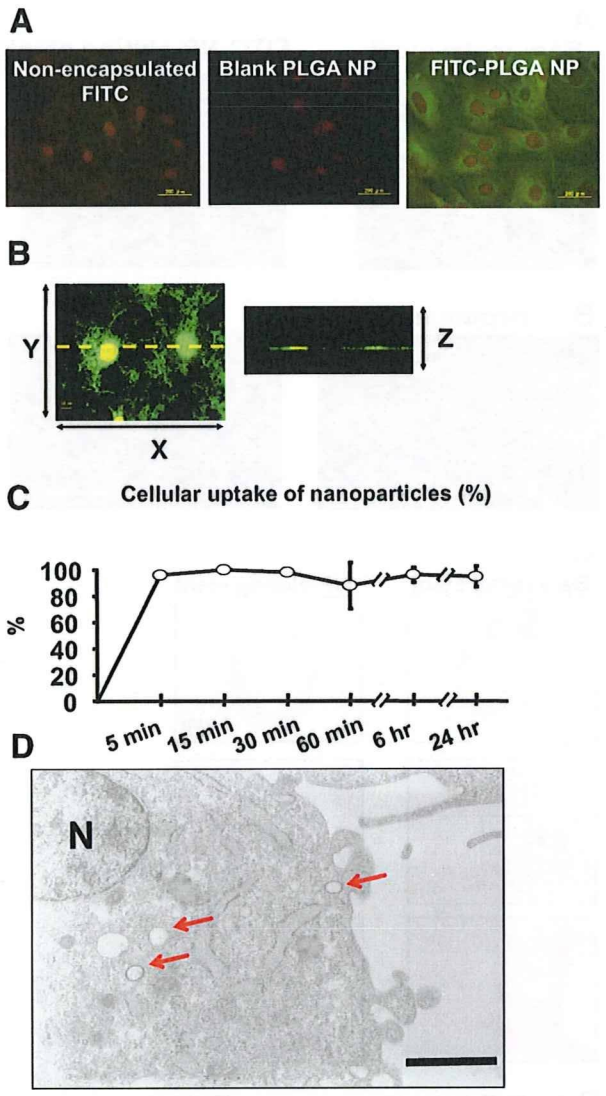

Figure 2. Cellular Uptake and Intracellular Distribution of NP in Human Coronary Artery SMCs In Vitro

(A) Fluorescence microscopy photographs of human coronary artery smooth muscle cells (SMCs) incubated with FITC only, blank NP, or FITC-NP (0.1 mg/ml) for 1 h. **(B)** Confocal fluorescence microscopy photographs (**left**: an XY-axis image; **right**: a Z-axis image of cross-sections from **yellow dashed line** displayed on an XY-axis image) of human coronary artery SMCs incubated with FITC-NP at 0.1 mg/ml. The FITC fluorescence is **green**; nuclei are **red**. **Scale bar** = 10 μm. **(C)** In vitro time course of the percentage of cellular uptake of FITC-incorporated NP by human coronary artery SMCs (n = 6 to 8 at each time point). **(D)** Transmission electron microscopy photograph of a cross-section of human coronary artery smooth muscle incubated with NP for 60 min. **Arrows** indicate NP in the cellular cytoplasm. **Scale bar** = 500 nm. N = nucleus; PLGA = poly (DL-lactide-*co*-glycolide); other abbreviations as in Figure 1.

for 1 h, resulting in prominent cellular FITC positivity (Online Fig. IV A). In contrast, scarce FITC fluorescence was observed in the SMCs 1 h after addition of FITC-PLGA matrix eluted from PLGA polymer-based FITC-eluting stent (Online Fig. IV B).

Results of a cytotoxicity assay showed that human coronary artery SMCs incubated with PLGA NP for 48 h at concentrations of 0.1, 0.3, and 1 mg/ml remained 100% viable relative to control (data not shown).

Deployment of FITC-NP–eluting stent in porcine coronary arteries in vivo. After 1 week of stent deployment, a thin layer of platelets and fibrin deposition formed around the stent strut. Strong FITC fluorescence was detected in the stented coronary arterial segments that had received the FITC-NP–eluting stent (Fig. 3).

After 2 weeks, when a thin neointima associated with monocyte infiltration had formed mainly around stent struts, intense FITC fluorescence was detected in the stented coronary arterial segments from the NP-eluting stented groups (Fig. 4).

No substantial FITC fluorescence was observed in coronary segments from the non-NP polymer-based FITC stent site (Figs. 3 and 4) or from the bare metal stent sites (data not shown) 1 and 2 weeks after stenting.

After 4 weeks, when a significant in-stent neointima formed in stent sites and the neointima consisted mainly of VSMCs, FITC fluorescence was noted only in cross-sections from the NP-eluting stent site but not from bare metal stent sites (Fig. 5A). No substantial FITC fluorescence was observed in cross-

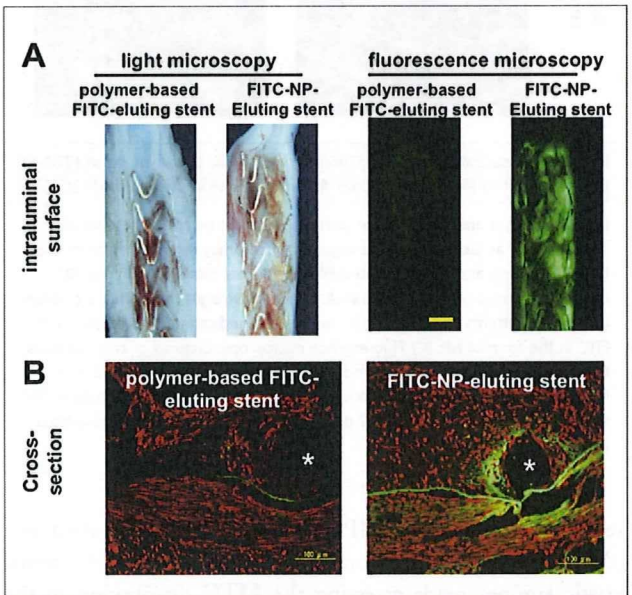

Figure 3. Localization of FITC Fluorescence After Deployment of FITC-NP–Eluting Stent in Porcine Coronary Arteries 1 Week After Stenting

(A) En-face light and fluorescence stereomicroscopic pictures of the intraluminal surface of an isolated stented segment of coronary artery taken from the FITC-NP–eluting and the polymer-based FITC-eluting stent sites. **Scale b** = 1 mm. **(B)** Fluorescence microscopic pictures of cross-sections from the FITC-NP–eluting stent and polymer-based FITC-eluting stent sites. Microscopic settings (exposure condition, filter, intensity of excitation light, and so forth) are the same between 2 pictures. **Scale b** = 100 μm. Abbreviations as in Figure 1.

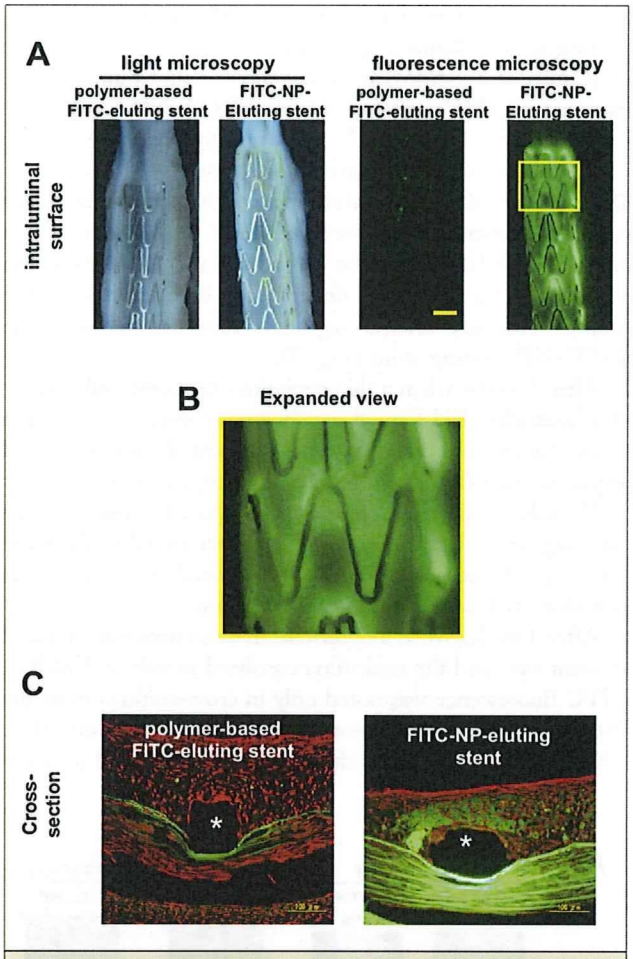

Figure 4. Localization of FITC Fluorescence After Deployment of FITC-NP–Eluting Stent in Porcine Coronary Arteries 2 Weeks After Stenting

(A) En-face light and fluorescence stereomicroscopic pictures of the intraluminal surface of an isolated stented segment of coronary artery taken from the FITC-NP–eluting and the dip-coated FITC stent sites. **Scale b** = 1 mm. **(B)** Expanded images of **boxed area in A**. Expanded images reveal that a number of discrete patterns of fluorescence can be seen, indicating local retension of FITC in the form of NP. **(C)** Fluorescence microscopic pictures of cross-sections from the FITC-NP–eluting stent and polymer-based FITC-eluting stent sites. Microscopic settings (exposure condition, filter, intensity of excitation light, and so forth) are the same between 2 pictures. **Scale b** = 100 μm. Abbreviations as in Figure 1.

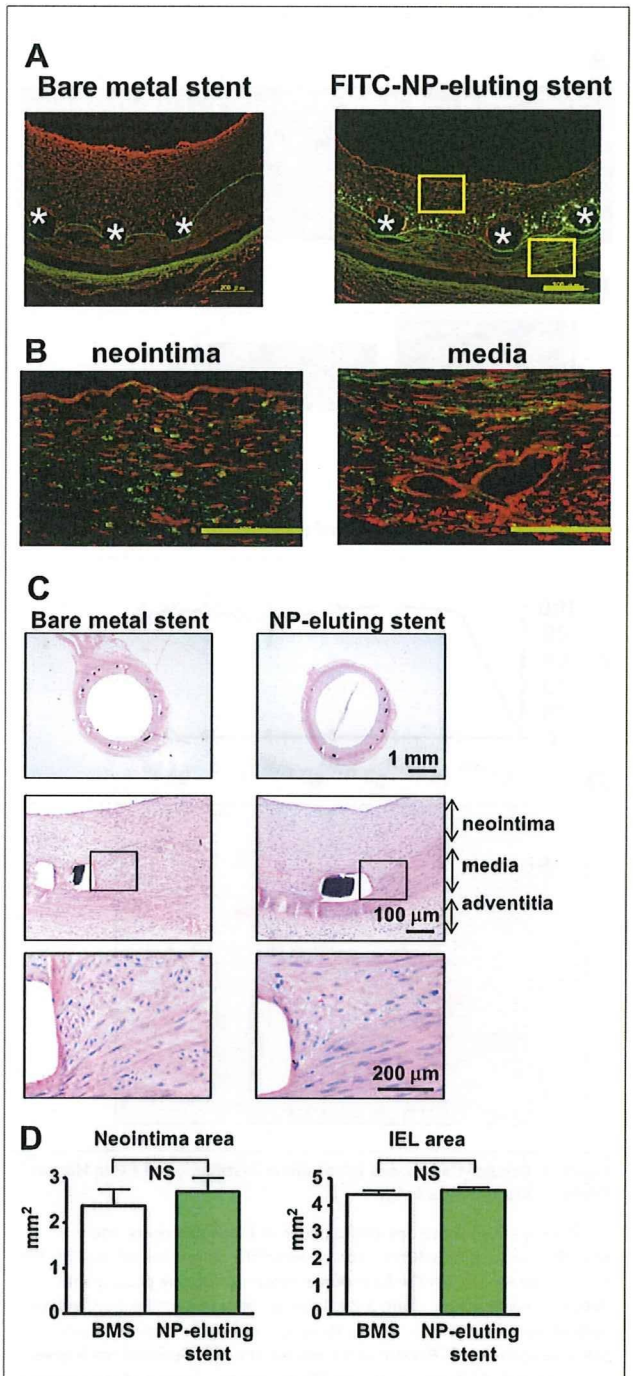

Figure 5. Localization of FITC Fluorescence and Histopathology in Porcine Coronary Artery 4 Weeks After Stenting

(A) Fluorescence microscopy photographs of cross-sections from bare-metal stent (BMS) and NP-eluting stent sites. **Scale b** = 100 μm. **(B)** Expanded images of neointima and media from boxed areas in **(A)**. **(C)** Representative low- **(upper panels)**, middle- **(middle panels)**, and high-magnification **(lower panels)** photomicrographs of hematoxylin-eosin stained sections of coronary arteries after 4 weeks from coronary artery segments that received BMS and the NP-eluting stents. **(D)** The neointimal area and the area within the internal elastic lamina (IEL) at the BMS and the NP-eluting stent sites (n = 6 each). *site of stent strut. Abbreviations as in Figure 1.

sections from the non-NP polymer-based FITC stent site (data not shown). Autofluorescence of the internal and external elastic laminas made assessing the FITC distribution in the neointima and media possible. The neointima and media around the stent strut expressed intense fluorescence, whereas a discrete and circular-shaped fluorescence was noted in cells of either layer distal to the stent strut (Fig. 5B). Fluorescence-positive cell counts revealed that cellular FITC positivity was 90 ± 12% and 76 ± 10% (n = 8), in the neointima and the media, respectively. Adventitial delivery was more difficult to quantify, due to the presence of autofluorescence. After 6

JACC: CARDIOVASCULAR INTERVENTIONS, VOL. 2, NO. 4, 2009
APRIL 2009:277–83

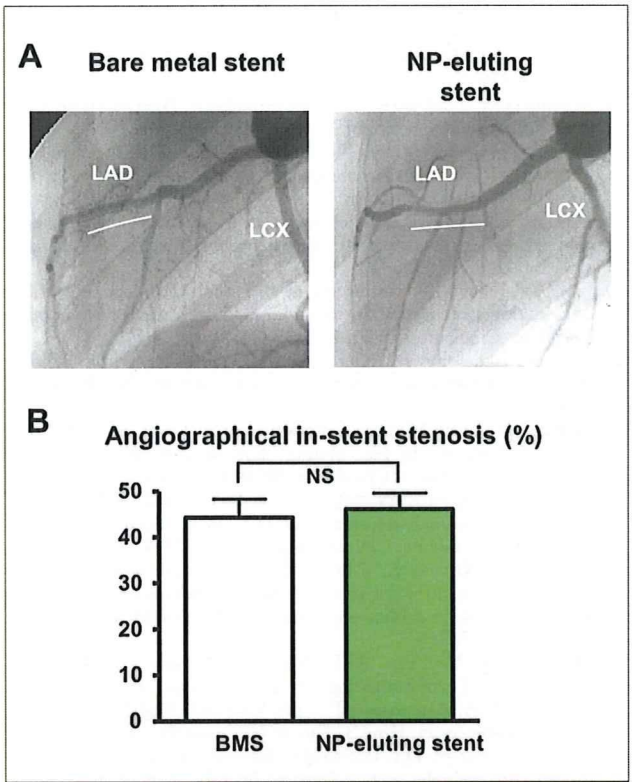

Figure 6. Coronary Arteriography and In-Stent Stenosis

(A) Representative coronary arteriographic images 4 weeks after nanoparticle (NP)-eluting stent and bare-metal stent (BMS) implantation. **White bars** in the images denote stent segment sites. **(B)** Angiographic in-stent stenosis 4 weeks after NP-eluting stent site (n = 8) and BMS site (n = 8). LAD = the left anterior descending coronary artery; LCX = left circumflex coronary artery.

weeks, cellular FITC signal declined spontaneously (cellular FITC positivity was <10% in the neointima and media, data not shown).

In hematoxylin-eosin stained sections, there were no significant differences in the degrees of inflammation among the 3 groups after 4 weeks (Fig. 5C, Online Fig. V, and Online Table). A significant in-stent neointima was formed in the non-coated bare metal stent and NP-eluting stent sites, and the neointima consisted mainly of VSMC. Quantitative analysis of the neointima after 4 weeks revealed no significant differences in neointima formation, stent area, or medial area between the 2 groups (Fig. 5D). In addition, angiographically examined in-stent stenosis was comparable between the 2 groups (Fig. 6).

Discussion

We present the first NP-eluting stent formulated with a newly invented cation electrodeposition coating technology as an excellent drug delivery platform. Importantly, this NP-mediated DDS is able to carry hydrophilic agents such as FITC (15,17), which offers advantages over the current stent-coating technology (see also introductory text). The PLGA is a bioabsorbable polymer with a long history of safe use in medical applications. For clinical use, PLGA-NP can be manufactured in pyrogen-free form under the good manufacture practice guidelines.

Characteristics of NP-eluting stent. To create a cationic electrodeposition coating, NP surface was rendered cationic with chitosan-mediated surface-modification (16). This cationization offers several advantages. Firstly, compared with anionic NP, cationic NP increases the intracellular incorporation rate of NP. Secondly, it accelerates the escape of entrapped NP from the endosomal compartment to cytoplasmic compartment. This escape is important, because therapeutic agents (drug, protein, DNA, and the like) are prone to destabilize in the endosomal compartment. Thirdly, NP retained in the cytoplasm or extracellular spaces release encapsulated drug slowly in conjunction with the hydrolysis of PLGA-NP and diffusion from NP. The slow intracellular release might result in sustained intracellular drug delivery. It is likely that these advantages contribute to the highly efficient delivery of NP eluted from the NP-eluting stent into the neointima and media in vitro (Fig. 2, Online Fig. IV) and in vivo (Figs. 3 to 5). Because FITC is hydrophilic and free FITC released from FITC-encapsulated NP must be washed out rapidly, a considerable part of small circular shaped fluorescence might come from NP still containing FITC within the cell or in extracellular spaces. The FITC release kinetics from the NP-eluting stent supports this notion. In contrast, prior reports showed that the intracellular drug/gene delivery capacity of stents coated with polymer and water-soluble drug/gene is limited (10,11); drug/gene delivery persisted for up to 7 days, and the percentage of positive cells ranged from 1% to 2%. Therefore, our present NP-eluting stent system is a more efficient DDS than those created with non-NP polymeric DES coating technology. Recently, we found that NP-eluting stents could deliver other water-soluble agents such as oligonucleotide or plasmid DNA into porcine coronary arteries (Drs. Nakano K and Egashira K, unpublished observations, May 2007). Therefore, our NP-eluting stent system provides an innovative platform for delivering therapeutic agents in the future treatment of cardiovascular diseases.

Clinical implication. Evidence of impaired arterial healing process is a major histopathological feature in the arteries of experimental animals (18,19) and humans (8,9) exposed to DES in current use. Therefore, it is important to consider potential toxicities associated with the delivery of PLGA NP from an NP-eluting stent system. Of a number of polymer matrix materials evaluated for stent coating, it has been shown that PLGA do not increase the incidence of thrombosis in a porcine coronary artery model (18). Our NP-eluting stents had no apparent effect on stent-induced injury, inflammation, or endothelial regeneration in vivo, suggesting that PLGA NP transfer to the arterial wall does not impair the arterial healing

process in this model. Overall, these data of vascular compatibility support the notion that this bioabsorbable PLGA NP-eluting stent system could be applied to human subjects without vascular toxicity.

Efficacy studies in animals are needed to determine the therapeutic potential of this NP-eluting stent system. Potential therapeutic strategies for this stent-based platform include the delivery of proteins or genes that inhibit inflammation, SMC proliferation, and thrombosis. We plan to examine the effects of antimonocyte chemoattractant protein-1 (13,20–22) or nuclear factor κ-B (12) delivered via the NP-eluting stent. Furthermore, it would be interesting to deliver multiple agents with different time courses from 1 NP-eluting stent. The bioabsorbtion time of PLGA in living body is controlled by molecular make-up of PLGA (the ratio of D,L-lactic acid and glycolic acid) (23), allowing us to modulate the time course of intracellular drug delivery. Finally, cell-specific delivery of NP into VSMC to suppress neointima formation or into endothelial cells to accelerate endothelial regeneration might be attractive strategies. Future studies will test the feasibility of each of these innovative approaches.

Conclusions

These data suggest that this bioabsorbable polymeric NP-eluting stent system has unique aspects in novel electrodeposition coating technology, vascular compatibility, and an efficient DDS (better and more prolonged delivery of FITC into the stented coronary artery), compared with dip-coated polymer-eluting stent. This system might hold promise as an innovative platform for the delivery of less invasive nano-devices targeting cardiovascular disease. Further efficacy and good laboratory practice-compliant safety studies are needed to prove this notion.

Acknowledgments

The authors would like to thank E. Iwata and M. Miyagawa for their excellent technical assistance.

Reprint requests and correspondence: Dr. Kensuke Egashira, Department of Cardiovascular Medicine, Graduate School of Medical Science, Kyushu University, 3-1-1, Maidashi, Higashi-ku, Fukuoka 812-8582, Japan. E-mail: egashira@cardiol.med.kyushu-u.ac.jp.

REFERENCES

1. Babapulle MN, Eisenberg MJ. Coated stents for the prevention of restenosis: Part I. Circulation 2002;106:2734–40.
2. Babapulle MN, Eisenberg MJ. Coated stents for the prevention of restenosis: Part II. Circulation 2002;106:2859–66.
3. Serruys PW, Kutryk MJ, Ong AT. Coronary-artery stents. N Engl J Med 2006;354:483–95.
4. Laskey WK, Yancy CW, Maisel WH. Thrombosis in coronary drug-eluting stents: report from the meeting of the Circulatory System Medical Devices Advisory Panel of the Food and Drug Administration Center for Devices and Radiologic Health, December 7–8, 2006. Circulation 2007;115:2352–7.
5. Shuchman M. Debating the risks of drug-eluting stents. N Engl J Med 2007;356:325–8.
6. Shuchman M. Trading restenosis for thrombosis? New questions about drug-eluting stents. N Engl J Med 2006;355:1949–52.
7. Luscher TF, Steffel J, Eberli FR, et al. Drug-eluting stent and coronary thrombosis: biological mechanisms and clinical implications. Circulation 2007;115:1051–8.
8. Finn AV, Nakazawa G, Joner M, et al. Vascular responses to drug eluting stents. Importance of delayed healing. Arterioscler Thromb Vasc Biol 2007;27:1500–10.
9. Finn AV, Joner M, Nakazawa G, et al. Pathological correlates of late drug-eluting stent thrombosis: strut coverage as a marker of endothelialization. Circulation 2007;115:2435–41.
10. Klugherz BD, Jones PL, Cui X, et al. Gene delivery from a DNA controlled-release stent in porcine coronary arteries. Nat Biotechnol 2000;18:1181–4.
11. Walter DH, Cejna M, Diaz-Sandoval L, et al. Local gene transfer of phVEGF-2 plasmid by gene-eluting stents: an alternative strategy for inhibition of restenosis. Circulation 2004;110:36–45.
12. Ohtani K, Egashira K, Nakano K, et al. Stent-based local delivery of nuclear factor-kappaB decoy attenuates in-stent restenosis in hypercholesterolemic rabbits. Circulation 2006;114:2773–9.
13. Egashira K, Nakano K, Ohtani K, et al. Local delivery of anti-monocyte chemoattractant protein-1 by gene-eluting stents attenuates in-stent stenosis in rabbits and monkeys. Arterioscler Thromb Vasc Biol 2007;27:2563–8.
14. Wickline SA, Neubauer AM, Winter P, Caruthers S, Lanza G. Applications of nanotechnology to atherosclerosis, thrombosis, and vascular biology. Arterioscler Thromb Vasc Biol 2006;26:435–41.
15. Niwa T, Takeuchi H, Hino T, Kunou N, Kawashima Y. In vitro drug release behavior of D,L-lactide/glycolide copolymer (PLGA) nanospheres with nafarelin acetate prepared by a novel spontaneous emulsification solvent diffusion method. J Pharm Sci 1994;83:727–32.
16. Yamamoto H, Kuno Y, Sugimoto S, Takeuchi H, Kawashima Y. Surface-modified PLGA nanosphere with chitosan improved pulmonary delivery of calcitonin by mucoadhesion and opening of the intercellular tight junctions. J Control Release 2005;102:373–81.
17. Panyam J, Zhou WZ, Prabha S, Sahoo SK, Labhasetwar V. Rapid endo-lysosomal escape of poly(DL-lactide-co-glycolide) nanoparticles: implications for drug and gene delivery. Faseb J 2002;16:1217–26.
18. van der Giessen WJ, Lincoff AM, Schwartz RS, et al. Marked inflammatory sequelae to implantation of biodegradable and nonbiodegradable polymers in porcine coronary arteries. Circulation 1996;94:1690–7.
19. Lincoff AM, Furst JG, Ellis SG, Tuch RJ, Topol EJ. Sustained local delivery of dexamethasone by a novel intravascular eluting stent to prevent restenosis in the porcine coronary injury model. J Am Coll Cardiol 1997;29:808–16.
20. Ohtani K, Usui M, Nakano K, et al. Antimonocyte chemoattractant protein-1 gene therapy reduces experimental in-stent restenosis in hypercholesterolemic rabbits and monkeys. Gene Ther 2004;11:1273–82.
21. Egashira K, Zhao Q, Kataoka C, et al. Importance of monocyte chemoattractant protein-1 pathway in neointimal hyperplasia after periarterial injury in mice and monkeys. Circ Res 2002;90:1167–72.
22. Egashira K. Molecular mechanisms mediating inflammation in vascular disease: special reference to monocyte chemoattractant protein-1. Hypertension 2003;41:834–41.
23. Miller RA, Brady JM, Cutright DE. Degradation rates of oral resorbable implants (polylactates and polyglycolates): rate modification with changes in PLA/PGA copolymer ratios. J Biomed Mater Res 1977;11:711–9.

Key Words: drug delivery system ■ nanotechnology ■ restenosis ■ smooth muscle cells ■ stents.

APPENDIX

For a supplementary Methods section and supplementary figures, please see the online version of this article.

Online Appendix for the following

April *JACC: Cardiovascular Interventions* article

TITLE: Formulation of Nanoparticle-Eluting Stents by a Cationic Electrodeposition Coating Technology: Efficient Nano-Drug Delivery via Bioabsorbable Polymeric Nanoparticle-Eluting Stents in Porcine Coronary Arteries

AUTHORS: Kaku Nakano, PHD, Kensuke Egashira, MD, PHD, Seigo Masuda, MD, Kouta Funakoshi, MD, Gang Zhao, MD, PHD, Satoshi Kimura, MD, Tetsuya Matoba, MD, PHD, Katsuo Sueishi, MD, PHD, Yasuhisa Endo, PHD, Yoshiaki Kawashima, PHD, Kaori Hara, PHD, Hiroyuki Tsujimoto, PHD, Ryuji Tominaga, MD, PHD, Kenji Sunagawa, MD, PHD

APPENDIX

Methods

Preparation of cationic PLGA NP with surface modification with chitosan

A lactide/glycolide copolymer (PLGA) with an average molecular weight of 20,000 and a copolymer ratio of lactide to glycolide of 75:25 (PLGA7520; Wako Pure Chemical Industries, Osaka, Japan) was used as a wall material for the NP. According to manufacturer's instruction, a bioabsorption half-life of this product is 2 weeks in rat tissue.[1] Chitosan (Mw. 50,000; deacetylation degree 80%; Katakurachikkarin, Tokyo,

Japan) was used to coat the surface of PLGA NP. Polyvinylalcohol (PVA-403; Kuraray, Osaka, Japan) was used as a dispersing agent. Fluorescein-isothiocyanate (FITC; Dojindo laboratories, Kumamoto, Japan), a water-soluble reagent, was used as a fluorescent marker of the NP. PLGA NP encapsulated with FITC was prepared by a previously reported emulsion solvent diffusion method in purified water. PLGA (2 g) were dissolved in a mixture of acetone (40 ml), ethanol (20 ml). Then, FITC (100 mg) was added into this solution. The resultant polymer-FITC solution was emulsified in PVA and chitosan solution under stirring at 400 rpm using the propeller-type agitator with four blades. After agitating the system for about 1 h under reduced pressure at 40 °C, the entire suspension was centrifuged (41,000 x *g* for 20 min at -20 °C). After removing the supernatant, purified water was added to mix with the sediment. The wet mixture was then centrifuged again to remove the excess PVA and the unencapsulated reagent that could not adsorb on the surfaces of NP. After repeating this process, the resultant dispersion was freeze-dried under the same conditions (See online Figure IA).

The mean particle size was analyzed by light scattering method (Microtrack UPA150; Nikkiso, Tokyo, Japan). A sample of nanoparticulate suspension in distilled water was used for particle size analysis. An average particles size of 241.6 nm (D10 = 147.2 nm, D90 = 284.1 nm) with a narrow size distribution (see online Figure IB). The FITC-encapsulated PLGA NP contained 5 % FITC. The zeta potential of the NP as measured by Zetasizer Nano Z (Malverm, America) was +6.7 mV.

Preparation of NP-eluting stent by a cationic electrodeposition coating technology

A 15-mm-long stainless-steel, balloon-expandable stents (Multilink, Guidant) were

ultrasonically cleaned by acetone, ethanol (70%), and demineralized water. Cationic electrodeposition coating was prepared on cathodic stents in PLGA NP solution at a concentrations of 50 mg/mL in distilled water with current maintained at 2.0 mA by a direct current power supply (DC power supply, Nippon Stabilizer Co, Tokyo, Japan) for different period under sterile conditions (illustrative explanation in next page). The coated stents were-dried vacuously overnight. This electrodeposition coating procedure produced a coating of approximately 654 ± 168 μg of NP per stent and 31 ± 2 μg of FITC per stent (n= 12). Surface of some NP-coating stents were observed with scanning electron microscopy (JXM8600, JEOL, Tokyo, Japan).

As control, dip-coated stents with thin layers of PLGA polymer, containing about 600 μg of PLGA polymer and 30 μg of FITC, were prepared as we previously described [2]. Prior to experimental use, non-coated bare metal and NP-coated stents were mounted over the 3-mm balloon for implantation in the coronary artery. These balloon mounted stent sets were sterilized using ethylene oxide gas.

Schematic illustration of the electrodeposition coating system (chamber, electrodes, and DC power supply) for a cation nanoparticle coating technology. Three steps of electrodeposit coating procedure are shown in online Figure II.

Measurement of *in vitro* release kinetics

To measure NP release kinetics *in vitro*, the FITC-NP-coated stents (n=8) were immersed in Tris-EDTA buffer, and the FITC containing NP that was subsequently eluted into the buffer was measured using a fluorescence plate reader (Mithras LB 940-AS, Berthold Technologies, Bad Wildbad, Germany) at excitation and emission wavelengths of 480 and 525 nm, respectively. To measure FITC release kinetics, FITC-NP (n = 8) were immersed in Tris-EDTA buffer, and the released FITC from NP was measured.

Cellular uptake and intracellular distribution of nanoparticles

Human coronary artery smooth muscle cells (SMCs) were obtained from Cambrex Bio Science Walkersville, Inc. and cultured in SmGM-2 (Cambrex Bioscience, Charles City, IA). Each cell was used between passages 4 to 8.

The SMCs were seeded on 48-well culture plate to an initial concentration of 1 x 10^5 cells per well and incubated at 37 °C/5 % CO_2 environment until cells were subconfluent. The growth medium was replaced with the FITC-loaded PLGA nanoparticles suspension medium (0.1 to 0.5 mg/mL) and then further incubated for 1 hour. The cells were then washed three times with PBS to eliminate extracellular nanoparticles which were not incorporated into the cells. Then, the cells were fixed with 1 % formaldehyde/PBS buffer and nuclear was counterstained with propidium iodide.

Cellular uptake of FITC-loaded PLGA NP was evaluated by confocal fluorescence microscopy. The images were digitized and analyzed with Adobe Photoshop and Scion Image Software. The total number of fluorescence positive cells in each field and the number of total cells was counted. Cellular uptake percentage was assessed by the percentage of fluorescence positive cells per total cells in each field. In part of experiment, the internal properties of NP were examined by transmission electron microscopy (H-7000E, Hitachi, Tokyo, Japan).

Cytotoxicity assay

The cytotoxicity of PLGA nanoparticles on human coronary artery SMCs was determined using a MTS assay (Cell Counting Kit-8, Dojindo Inc., #343-07626). The cells were grown in 96-well microtiter plates for 24 hours, and then they were treated with different concentrations of FITC-loaded PLGA nanoparticles suspension medium with 10 % FBS. The plates were incubated for 48 hours and then the medium was replaced with 200 μl of fresh medium. Next, 2 mg/ml MTS solution was added and the plates were incubated again for 4 hours at 37°C/5%CO_2. Finally, absorbance was measured at 490 nM using an enzyme-linked immunosorbent assay reader. Cell viability was expressed as the ratio between the amount of formazan determined for cells treated with PLGA nanoparticles and for control non-treated cells.

Animal Preparation and Stent implantation

The animal-model experiments were reviewed and approved by the Committee on Ethics on Animal Experiments, Kyushu University Faculty of Medicine, and were performed

according to the guidelines of the National Institutes of Health (NIH) Guide for the Care and Use of Laboratory Animals. Domestic male pigs (Kyudo, Tosu, Japan; aged 2 to 3 months and weighing 25 to 30 kg) were used.

Animals were anesthetized and divided into 3 groups, which underwent deployment of either a non-coated bare metal stents (1 week, n = 3; 2 week, n=3; 4 week, n = 8; 6 week, n = 3), FITC-incorporated NP-eluting stents (2 week, n = 3; 2 week, n=3; 4 week, n= 8; 6 week, n = 3), or dip-coated stents with thin layers of PLGA polymer containing FITC (1 week; n=3, 2 week; n=3, 4 week; n=3), to either the left anterior descending (LAD) or the left circumflex coronary (LCx) arteries. After arterial blood samples were taken, animals were euthanized with a lethal dose of anesthesia after 1, 4, or 6 weeks, and the stented arterial sites and contralateral non-stented sites were excised for biochemical, immunohistochemical, and morphometric analyses.

A segment with a mean coronary diameter of 2.5 mm was selected by using quantitative coronary angiography with a stent-to-artery ratio of approximately 1.1 to 1.2. A balloon catheter mounted with a stent was then advanced to the pre-selected coronary segments for deployment over a standard guide wire. The balloon catheter was inflated at 15 atm for 60 seconds once and was then slowly withdrawn, leaving the stent in place. All animals received aspirin (330 mg/day) and ticlopidine (200 mg/day) until euthanasia from 3 days before stent implantation procedure.

Coronary Angiography

Left coronary angiography was performed before, immediately after, and 4 weeks after the stent implantation. A preshaped Judkins catheter was inserted into the right or left carotid artery, and coronary angiography in a left anterior oblique view was performed. Arterial pressure, heart rate, and ECG were continuously monitored and recorded on a recorder (Nihon Kohden, Tokyo, Japan).

Histopathological study

The left coronary artery was perfused with 10 % buffered formalin at 120 mm Hg and fixed for 24 hours. The stented artery segments were isolated and processed as described previously[2,3]: The segment was divided into two parts at the center of the stent, and the proximal part was embedded in methyl methacrylate mixed with *n*-butyl methacrylate to allow for sectioning through the metal stent struts. Serial sections were stained with elastica van Gieson or with hematoxylin-eosin (HE). The neointimal area, the area within the internal elastic lamina (IEL), and the lumen area were measured by computerized morphometry, which was carried out by a single observer who was blinded to the experimental protocol. All images were captured by an Olympus microscope equipped with a digital camera (HC-2500) and were analyzed using Adobe Photoshop 6.0 and Scion Image 1.62 Software. The injury and inflammatory scores were determined at each strut site, and mean values were calculated for each stented segment (Supplementary Table online). The extent of re-endothelialization was semi-quantitatively expressed as the percentage of circumference covered by the endothelium, as described previously. [4] The endothelialization score was defined as the extent of the circumference of the arterial